Numerical Validation of the Shear Compression Specimen. Part II: Dynamic Large Strain Testing

by A. Dorogoy and D. Rittel

ABSTRACT—Part I of this work addressed quasi-static loading of the shear compression specimen (SCS), which has been especially developed to investigate the shear dominant response of materials at various strain rates. The stress and strain states were characterized numerically. Approximations were presented to reduce the measured load, P, and displacement, d, into equivalent stress $\hat{\sigma}_{eq}$ and strain $\hat{\varepsilon}_{eq}$. This paper addresses dynamic loading of the SCS. Several simulations were made for representative materials, whose stress–strain behavior is assumed to be rate-independent. The results show that stress wave loading induces strong oscillations in the $P-d$ curve. However, the $\hat{\sigma}_{eq}-\hat{\varepsilon}_{eq}$ curve remains smooth in the gage section. The oscillations are about the quasi-static load values, so that with suitable filtering of the dynamic $P-d$ curves, the quasi-static ones are readily recovered. Consequently, the approach that was developed for quasi-static loading of the SCS is now extended to dynamic loading situations. The average strain rate is rather constant and scales linearly with the prescribed velocity. As the plastic modulus becomes smaller, the strain rate reaches higher values. Friction at the end pieces of the specimen is also investigated, and shown to have a small overall influence on the determined mechanical characteristics. This paper thereby confirms the potential of the SCS for large strain testing of materials, using a unified approach, over a large range of strain rates in a seamless fashion.

KEY WORDS—Large strain, shear compression specimen, elastic plastic material, finite elements, quasi-static, dynamic

Introduction

The determination of the dynamic mechanical properties, using specimens other than compression cylinders in a Kolsky apparatus,[1] is still the result of individual developments based on specific specimen geometry. When dynamic loading conditions, other than uniaxial tension[2] or compression, are applied, there are only very few specimens that are used on a "routine" basis. Dynamic shear testing of thin sheets was investigated by Rusinek and Klepaczko.[3] Very high strain rates in shear were achieved using a special pressure–shear plate impact experiment.[4] Shear testing (torsion) at high strain rates has been modeled using finite element technique by Gilat and Cheng[5] who investigated 1100 aluminum. Yet, among the various shear specimens available, perhaps the most popular is the "hat-specimen",[6] and its variation, the double-shear specimen.[7] These specimens are easily implemented in a Kolsky apparatus[1] or other type of dynamic loading system. Yet, in most cases, numerical simulations are required to validate the specimen, to determine the state of stress in the deformed gage, to analyze experimental results or to develop various new dynamic tests, such as adiabatic shear testing.[8] In this spirit, a new specimen geometry, the shear compression specimen (SCS), was proposed by Rittel et al.[9,10] to characterize the large strain material behavior over a large range of strain rates in a seamless manner. The specimen was first characterized using preliminary finite element simulations in the quasi-static context. Based on the quasi-static approximations, as well as experimental validations, the SCS was successfully used to study actual materials.[11] A detailed numerical study of the SCS subjected to quasi-static loading was presented in the first part of this paper in which basic issues were addressed.[12] This paper is the continuation of the first part, emphasizing now new dynamic aspects of the SCS. Several open issues are now systematically addressed, such as the influence of dynamic loading on the $P-d$ curve, and the uniformity of the stresses and strains in the mid-section of the gage. Another important issue is that of the attainable strain rates for the specimen geometry as a function of material parameters. The influence of frictional effects between the specimen end-pieces and the loading bars is also addressed, but the most important point is related to the procedure used to reduce dynamic $P-d$ curves into reliable $\hat{\sigma}_{eqv}-\hat{\varepsilon}_{eqv}$ curves. As will be shown in the following, the present study clearly demonstrates the previously developed quasi-static procedure can now be confidently applied to dynamic data reduction.

The paper is organized in four sections. This first section introduces the subject of this work. The second section deals with the investigation of the SCS subjected to dynamical loading. The results are discussed in the third section, and the conclusions are drawn in the fourth section.

The second section is divided into three subsections. Dynamic numerical solution schemes and assumptions are introduced in the first subsection. The numerical results are presented in the second subsection. These results include dynamic load–displacements curves, stress–strain curves, characterization of the average strain rate, and the assessment of frictional effects from the end-pieces of the SCS. The third subsection is dedicated to a validation exercise aimed at showing that the quasi-static procedure applies to the dynamic case as well.

A. Dorogoy is a Postdoctoral Fellow and D. Rittel (SEM Member, meritel@tx.technion.ac.il) is an Associate Professor, Mechanical Engineering Department, Technion—Israel Institute of Technology, 32000, Haifa, Israel.

Original manuscript submitted: July 6, 2004.
Final manuscript received: January 4, 2005.
DOI: 10.1177/0014485105052324

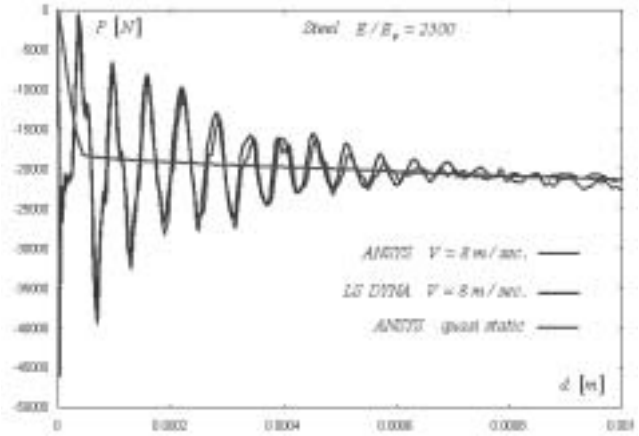

Fig. 1—The measured applied force P versus the applied displacement d for the quasi-static and dynamic ($v = 8$ m s^{-1}) types of loading and steel-like material

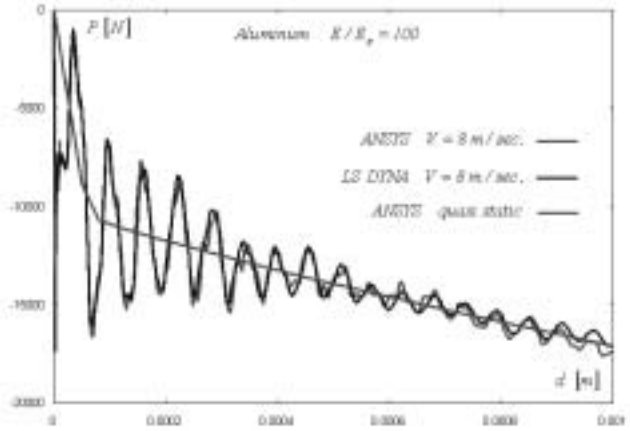

Fig. 2—The measured applied force P versus the applied displacement d for the quasi-static and dynamic ($v = 8$ m s^{-1}) types of loading and aluminum-like material

Investigation of the SCS Subjected to Dynamical Loading

Numerical Model

The SCS (see Fig. 1 of Part I[12]) was analyzed assuming dynamic loading. In order to verify the dynamic behavior of the SCS, we analyzed specimens made of two different materials (with mechanical properties similar to those of carbon steel and aluminum alloy). Two different constant velocities of 8 and 20 m s^{-1} were applied in the simulations. A key assumption was made, that the mechanical properties of these materials are strain-rate independent in order to pinpoint the differences between quasi-static and dynamic loading without the contribution of rate sensitivity. The length, diameter, gage thickness, width, and root corner radius were chosen to be $L = 20$ mm, $D = 10$ mm, $t = 2.5$ mm, $w = 2.0$ mm, and $R_1 = 0.4$ mm, respectively. The aluminum alloy-like material was assumed to be bilinear with Young's modulus $E = 73.8$ GPa, Poisson's ratio $\nu = 0.33$, yield stress $\sigma_Y = 400$ MPa and density $\rho = 2800$ kg m^{-3}. The carbon steel-like material was assumed to be bilinear with Young's modulus $E = 210$ GPa, Poisson's ratio $\nu = 0.3$, yield stress $\sigma_Y = 700$ MPa, and density $\rho = 7850$ kg m^{-3}. These two materials were chosen in order to represent the dynamic response of a wide spectrum of metal densities and Young's moduli.

The numerical analysis was carried out using the commercial finite element codes ANSYS and ANSYS LS-DYNA (Release 7.0, Ansys Inc.). The transient dynamic nonlinear equations were solved incrementally. The nonlinearity includes material and geometrical effects: plasticity and large strains. There are two methods for the solution of a transient problem:[13] the forward difference time integration method (implemented in LS-DYNA) and the Newmark time integration method (implemented in ANSYS). The forward difference method is used for explicit transient analyses, and the Newmark method is used for implicit transient analyses. The equation of motion was solved using both the implicit and the explicit schemes, and results were compared. Three-dimensional 10-Node Tetrahedral Structural Solid elements of type SOLID187 were used with ANSYS. Three-dimensional eight-node brick elements of type SOLID164 were used with LS-DYNA. The SOLID164 element uses reduced (one point) integration and viscous hourglass mode control.

To avoid meshing complications, the root corner radius of the SCS gage was assumed to be zero (sharp corner) in the LS-DYNA analyses. Due to the symmetry of the problem, only one-half of the specimen was again modeled. The boundary conditions of the dynamic problem are identical to those applied in the quasi-static case, except for a prescribed velocity instead of displacement. Constant velocities of $v = 8.0$ and 20.0 m s^{-1} were applied for $t = 125$ and 50 μs, respectively, resulting in a total displacement of $d = 1$ mm. These velocities are comparable to those applied in a typical dynamic test in which the SCS is loaded by means of a split Hopkinson pressure bar.[1]

Results

Load-Displacement Curves

The resulting P (reaction) versus applied d (displacement) curves are plotted in Figs. 1–3. These two parameters are measured during a typical experiment, whether quasi-static or dynamic. The $P - d$ curve of a steel-like specimen made of the material, with $E/E_p = 2500$, loaded at 8 m s^{-1}, is shown in Fig. 1. The quasi static $P - d$ is also plotted for comparison. Figure 1 reveals a significant difference between the static and dynamic loading situations. Since stress waves propagate through the specimen during dynamic loading, the resulting measured force oscillates strongly. The oscillations are evident in the elastic and plastic regions, and they tend to decrease with time. A very good agreement can be noted between the results obtained by the implicit and explicit solution schemes.

The $P - d$ curve of an aluminum-like specimen with $E/E_p = 100$ is shown in Figs. 2 and 3. These curves correspond to prescribed velocities of 8 and 20 m s^{-1}, respectively. In both figures, the quasi-static $P - d$ curves are plotted for comparison. Again, a very good agreement is observed between the results obtained by the implicit and the explicit schemes. Comparing Figs. 1–3, we observe the same

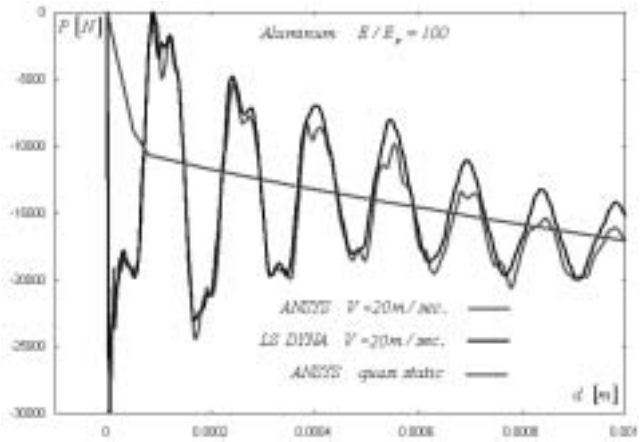

Fig. 3—The measured applied force P versus the applied displacement d for the quasi-static and dynamic (v = 20 m s^{-1}) types of loading and aluminum-like material

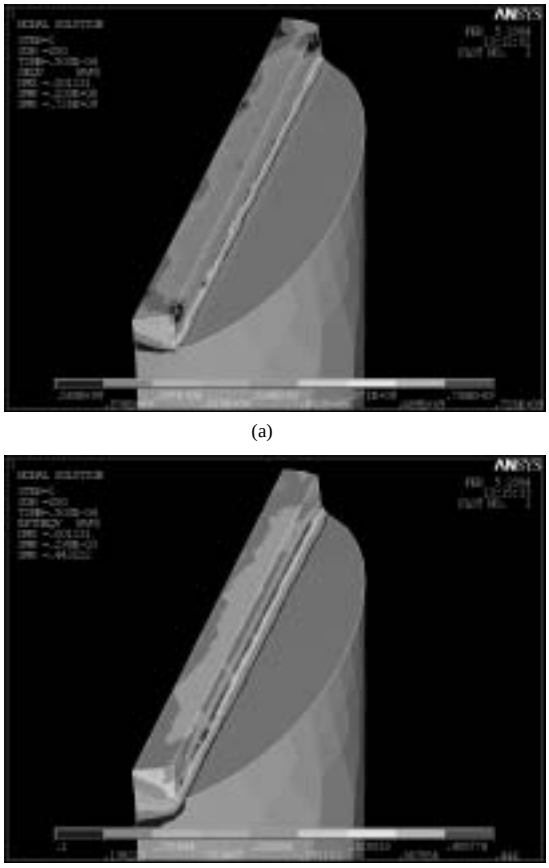

(a)

(b)

Fig. 4—Variation of $\hat{\sigma}_{eqv}$ and $\hat{\varepsilon}_{eqv}$ for E / E_p = 100 loaded at 20 m s^{-1} at d = 1 mm: (a) variation of $\hat{\sigma}_{eqv}$ on the mid-section; (b) variation of $\hat{\varepsilon}_{eqv}$ on the mid-section

strong oscillations of the load, irrespective of the material or prescribed velocity. Since the longitudinal wave speed of both materials is quite similar, the number of wave reflections that develop during the 125 μs of the loading is similar.

It can be observed in Fig. 3 that increasing the prescribed velocity yields stress waves of higher amplitude. As the loading duration at 20 m s^{-1} is of 50 μs, the number of wave reflections is smaller in comparison with the 125 μs of loading of Fig. 2.

However, an essential characteristic of the load oscillations is that the dynamic load oscillates about the quasi-static load values. In other words, keeping in mind that the mechanical properties were assumed to be strain-rate insensitive, it is easily observed that by suitable filtering of the dynamic load–displacement curves, the quasi-static ones are readily recovered.

Stress–strain Curves

The distributions of σ_{eqv} and ε_{eqv} on the gage mid-section are shown in Figs. 4(a) and (b), respectively. In most of the section, σ_{eqv} lies in the range $0.94 \leq \sigma_{eqv}/\sigma_{eqv}^{max} \leq 1$, where σ_{eqv}^{max} is the maximum stress on this section. Concerning ε_{eqv}, we obtain that it lies in the range $0.88 \leq \varepsilon_{eqv}/\varepsilon_{eqv}^{max} \leq 1$, where ε_{eqv}^{max} is the maximum strain on this section. These results indicate a high degree of homogeneity of both σ_{eqv} and ε_{eqv}.

As shown above (Figs. 1–3), the results obtained by the explicit scheme are in very good agreement with the results obtained using the implicit scheme. Since the explicit scheme takes much less computer time, the dynamic analyses shown in the sequel were calculated using the explicit scheme.

The time variation of $\hat{\sigma}_{eqv}$ and $\hat{\varepsilon}_{eqv}$ in the mid-section during 50 μs of high velocity (20 m s^{-1}) loading is shown in Fig. 5 for the three different plastic moduli. Figures 5(a) ($\hat{\sigma}_{eqv}$) and (b) ($\hat{\varepsilon}_{eqv}$) clearly show that the gage section does not experience significant stress or strain oscillations, when compared with the $P - d$ curve (Figs. 1–3).

The $\hat{\sigma}_{eqv} - \hat{\varepsilon}_{eqv}$ curves of an aluminum-like specimen are plotted in Figs. 6 and 7, for three different plastic moduli, and prescribed velocities of 8 and 20 m s^{-1}, respectively. As before, the quasi-static $\hat{\sigma}_{eqv} - \hat{\varepsilon}_{eqv}$ curves are plotted as points for comparison. The lack of oscillations indicates that a state of dynamic equilibrium is rapidly established in the plastic regime in the gage section of relatively small dimensions. The resulting dynamic and quasi-static $\hat{\sigma}_{eqv} - \hat{\varepsilon}_{eqv}$ curves are therefore almost identical. Small differences occur for high loading speeds and very "soft" material. Figure 7 shows that for the case of $E/E_p = 2500$, the maximum dynamic stress and strain values corresponding to a displacement of 1 mm are $(\hat{\varepsilon}_{eqv}^{d}, \hat{\sigma}_{eqv}^{d}) = (0.33\,,\ 406.1$ MPa), whereas for quasi-static loading they are $(\hat{\varepsilon}_{eqv}^{s}, \hat{\sigma}_{eqv}^{s}) = (0.35\,,\ 402.1$ MPa). The differences are thus $\Delta_\varepsilon = (\hat{\varepsilon}_{eqv}^{d} - \hat{\varepsilon}_{eqv}^{s})/\hat{\varepsilon}_{eqv}^{s} = -6.1\%$ and $\Delta_\sigma = (\hat{\sigma}_{eqv}^{d} - \hat{\sigma}_{eqv}^{s})/\sigma_{eqv}^{s} = 1.0\%$. These differences are small, and for all practical purposes can be considered as negligible.

Given the smooth $\hat{\sigma}_{eqv} - \hat{\varepsilon}_{eqv}$ relationship in the gage itself, and its similarity to the quasi-static relationship, the following important conclusion is reached. The quasi-static analysis procedure that was developed to obtain the constitutive behavior can now be extended to the dynamic case, after suitable filtering of the $P - d$ curve.

On the Strain Rate

Typical evolutions of $\hat{\varepsilon}_{eqv}$ on the gage mid-section versus time, are presented in Fig. 8. These curves represent an

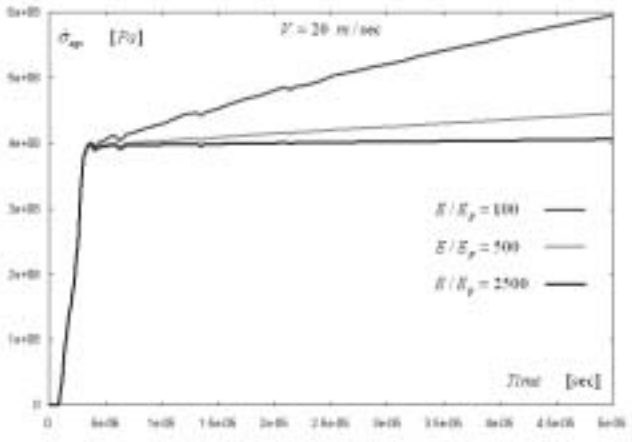

(a)

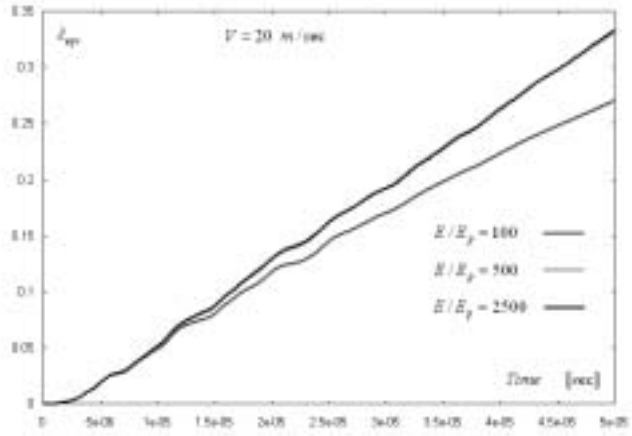

(b)

Fig. 5—$\hat{\sigma}_{eqv}$ and $\hat{\varepsilon}_{eqv}$ on the mid-section versus time for E / E_p = 100, 500, and 2500 loaded at 20 m s^{-1}: (a) $\hat{\sigma}_{eqv}$; (b) $\hat{\varepsilon}_{eqv}$

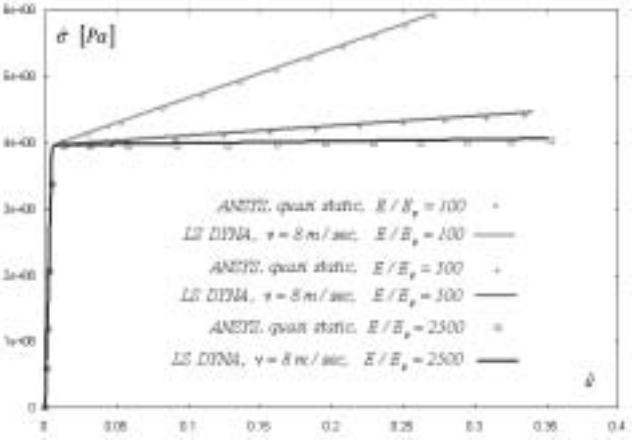

Fig. 6—$\hat{\sigma}_{eqv}$ on the mid-section versus $\hat{\varepsilon}_{eqv}$ for the quasi-static and dynamic (v = 8 m s^{-1}) types of loading

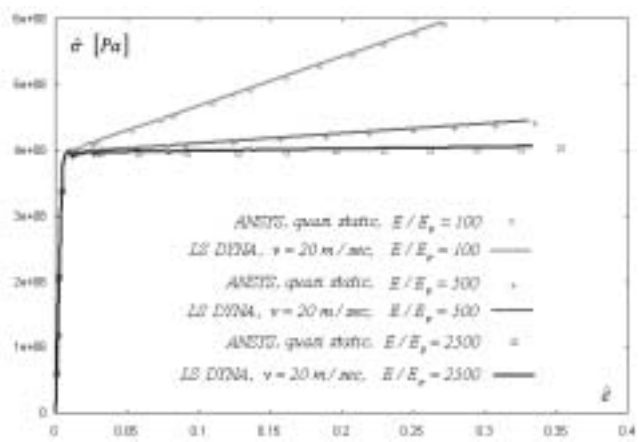

Fig. 7—$\hat{\sigma}_{eqv}$ on the mid-section versus $\hat{\varepsilon}_{eqv}$ for the quasi-static and dynamic (v = 20 m s^{-1}) types of loading

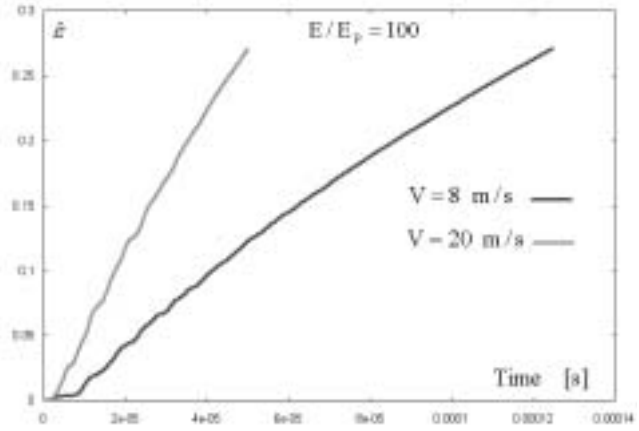

Fig. 8—$\hat{\varepsilon}_{eqv}$ on the mid-section versus time. The specimen is made of aluminum-like material with E / E_p = 100 loaded at velocities of v = 8 and 20 m s^{-1}

aluminum-like specimen with $E/E_p = 100$ loaded at 8 and 20 m s^{-1}, respectively. The slope of these curves is the strain rate, $\dot{\hat{\varepsilon}}_{eqv}$. The $\hat{\varepsilon}_{eqv} - t$ curves exhibit very small oscillations, so that for all practical purposes, the strain rate can be considered as constant throughout the test. The average strain rate, calculated by linear regression, is $\dot{\hat{\varepsilon}}_{eqv}$ = 2268 s^{-1}at 8 m s^{-1}, and $\dot{\hat{\varepsilon}}_{eqv}$ = 5694 s^{-1} at 20 m s^{-1}. These figures show that the average strain rate scales linearly with the prescribed velocity.

The effect of the plastic modulus on $\dot{\hat{\varepsilon}}_{eqv}$ is shown in Fig. 9. Aluminum-like specimens with sloth widths of w = 2 and 0.5 mm and three different plastic moduli, E/E_p = 100, 500, and 2500, were subjected to a prescribed velocity of 8 and 20 m s^{-1}, respectively. From Fig. 9(a), the averaged strain rates obtained for E/E_p = 100, 500, and 2500 are $\dot{\hat{\varepsilon}}_{eqv}$ = 2268, 2895, and 2965 s^{-1}, respectively. From Fig. 9(b), the averaged strain rates obtained for E/E_p = 100, 500, and 2500 are $\dot{\hat{\varepsilon}}_{eqv}$ = 8781, 13,769, and 15,939 s^{-1}, respectively. It can be observed that the smaller the plastic modulus, the higher the strain rate. It can also be observed that the smaller the slot width, the higher the strain rates achieved, as already observed in the quasi-static case.

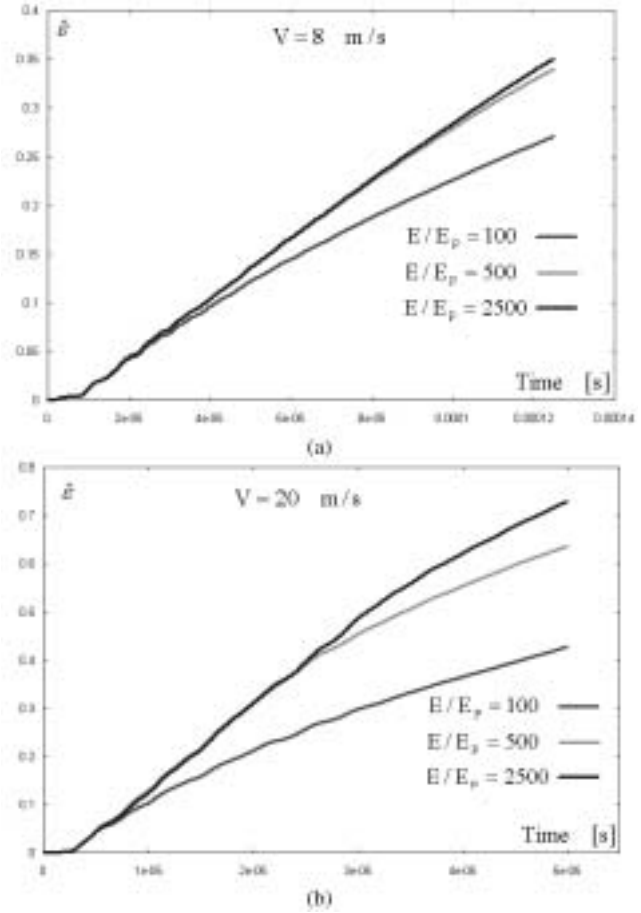

Fig. 9—The strain $\hat{\varepsilon}$ on the mid-section versus time. E / E_p = 100, 500, and 2500. (a) Aluminum-like specimen w = 2 mm subjected to v = 8 m s^{-1}. (b) Aluminum-like specimen with w = 0.5 mm subjected to v = 20 m s^{-1}

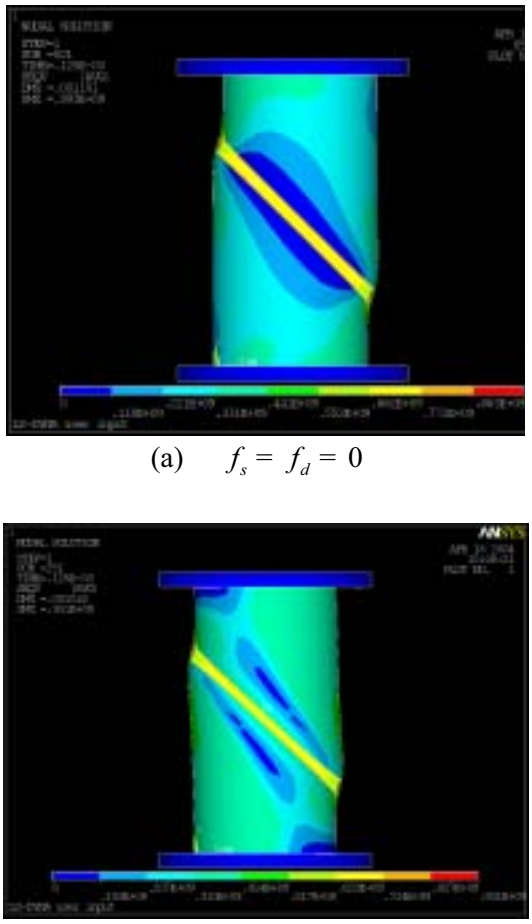

(a) $f_s = f_d = 0$

(b) $f_s = f_d = 0.25$

Fig. 10—The von Mises equivalent stress of an aluminum-like specimen confined between two rigid plates: (a) frictionless contact f = 0; (b) contact and friction f = 0.25

FRICTIONAL EFFECTS

Friction between the specimen end-pieces and the loading platens is an important issue that may affect the experimental results. Therefore, an aluminum-like specimen with $w = 1$ mm and $E/E_p = 100$ was confined between two rigid, 1 mm thick plates. The LS DYNA contact type "surface-to-surface" with contact option "automatic" was applied between the rigid disks and the specimen. The lower disk was fixed on its upper face by applying zero velocities. The upper disk was constrained to move only in the y direction by applying zero velocities in the x and z directions to its contact area. A constant velocity of 8 m s^{-1} was applied on its upper face for 125 μs, which resulted in a total displacement of $d = 1$ mm. Two coefficients of friction were considered: (1) frictionless contact $f_s = f_d = 0$, and (2) contact with friction $f_s = f_d = 0.25$.

Figure 10 represents the distribution of σ_{eqv} at $t = 125$ μs for each case. For frictionless contact, a contact slip condition exists between the upper disk and specimen, whereas for $f_s = f_d = 0.25$, a contact stick condition exists between the confining disks and specimen. These different contact conditions cause some changes to the overall stress picture, but the overall stress distribution in the specimen gage retains its homogeneity. Figure 10 also shows the deformed shape of the specimen in each case. Careful examination of the specimen boundaries reveals the lack of lateral motion of the specimen when friction operates. This visual indication may reveal the degree of frictional constraint operating during a test.

Figure 11 shows the distribution of σ_{eqv} on the mid-gage section, again at $t = 125$ μs. One can again note that the equivalent stress is homogeneous in both cases in this section. For the frictionless contact, $1.45 \leq \hat{\sigma}_{eqv}/\sigma_Y \leq 1.94$, while the stress state in most of the section is confined to $1.45 \leq \hat{\sigma}_{eqv}/\sigma_Y \leq 1.70$. For $f_s = f_d = 0.25$, we obtain $1.40 \leq \hat{\sigma}_{eqv}/\sigma_Y \leq 1.87$, while the stress state in most of the section is $1.40 \leq \hat{\sigma}_{eqv}/\sigma_Y \leq 1.64$. Therefore, frictionless contact causes slightly higher equivalent stresses.

Load–displacement curves are plotted in Fig. 12. Friction results in higher oscillations in the resulting load. Also, to apply a 1 mm displacement, a higher load needs to be applied in the frictional case. The load difference is of 13% between the frictional and frictionless case.

The $\hat{\sigma}_{eqv} - \hat{\varepsilon}_{eqv}$ curves are plotted in Fig. 13. In both cases the $\hat{\sigma}_{eqv} - \hat{\varepsilon}_{eqv}$ curves reproduce the assumed material model. However, the values of $\hat{\sigma}_{eqv}$ and $\hat{\varepsilon}_{eqv}$ in the presence

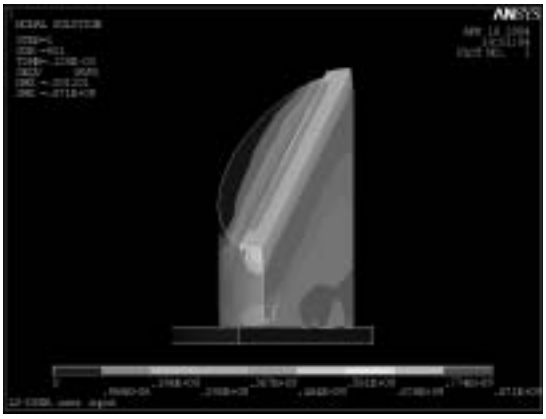

(a) $f_s = f_d = 0$

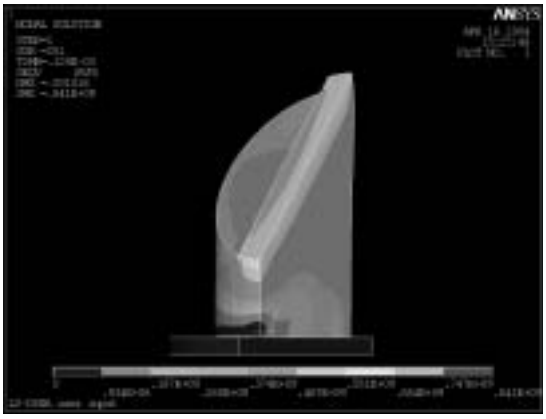

(b) $f_s = f_d = 0.25$

Fig. 11—The von Mises equivalent stress of an aluminum-like specimen in a section through the gage: (a) frictionless contact $f = 0$; (b) contact and friction $f = 0.25$

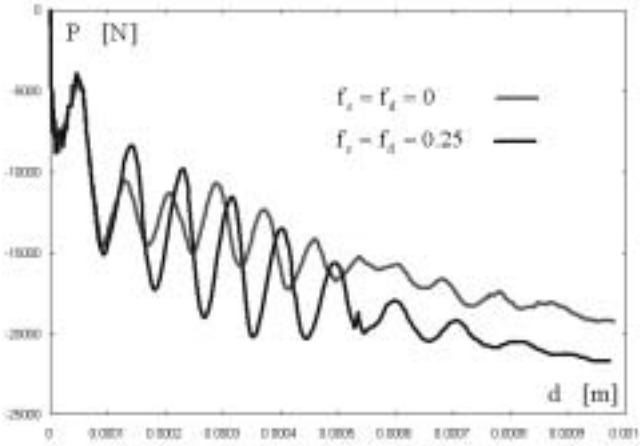

Fig. 12—A comparison of load–displacement curve for $f = 0$ and $f = 0.25$

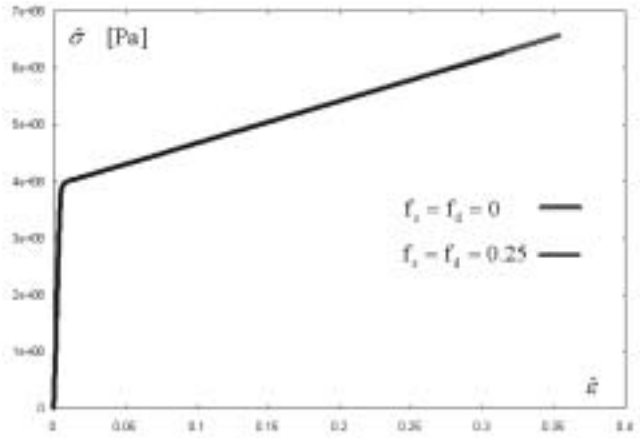

Fig. 13—A comparison of $\hat{\sigma}_{eqv} - \hat{\varepsilon}_{eqv}$ on the mid-section for $f = 0$ and $f = 0.25$

of friction are smaller. For a total applied vertical displacement of 1 mm, the difference in $\hat{\sigma}_{eqv}$ is ~5%, and for $\hat{\varepsilon}_{eqv}$, it is ~12%. Since stick and slip conditions are the two extreme conditions which might occur during an experiment, the above-mentioned differences may be considered as upper bounds. Therefore, care should be exercised to minimize frictional effects, as in any other mechanical test.

Verification Problem

In this section we verify that the quasi-static approximation is adequate to analyze dynamic $P - d$ curves when the oscillations of $\hat{\sigma}_{eqv} - \hat{\varepsilon}_{eqv}$ are smoothed.

First, an aluminum-like SCS with "unknown" yield stress $\sigma_Y = 450$ MPa and $E/E_p = 150$ is tested (numerically) in quasi-static loading and the three quasi-static coefficients are calculated. Then, the same aluminum-like SCS is tested dynamically (numerically) and the resultant $P - d$ curve is used as input "experimental data" to determine the dynamic $\hat{\sigma}_{eqv} - \hat{\varepsilon}_{eqv}$ curve by the quasi-static coefficients.

The three quasi-static coefficients, which were determined to process quasi-static $P - d$ curves of the specimen are $k_1 = 0.94$, $k_2 = 0.27$, and $k_3 = 0.85$. These coefficients are used with eqs (10) and (11) of Part I.[12] Substituting the "experimental" P and d along with the above-mentioned k, the $\hat{\sigma}_{eqv} - \hat{\varepsilon}_{eqv}$ curve is obtained, as shown in Fig. 14. The $\hat{\sigma}_{eqv} - \hat{\varepsilon}_{eqv}$ curve oscillates since the oscillations of the $P - d$ values were not smoothed or filtered at that stage. In order to eliminate these oscillations, least-squares fitting is used, as shown in Fig. 14 by a straight line. This straight line is supposed to estimate the real constitutive behavior of the material. The assumed constitutive relation is also plotted in Fig. 14. An excellent agreement is observed between the real values and those obtained by filtering the oscillating $\hat{\sigma}_{eqv} - \hat{\varepsilon}_{eqv}$ curve that was calculated using the quasi-static k. Hence, once determined, the k_i coefficients can be used to process all subsequent experimental data, whether dynamic or quasi-static. It may be noted that the constitutive behavior can be determined either by filtering the $P - d$ curve or by filtering the $\hat{\sigma}_{eqv} - \hat{\varepsilon}_{eqv}$ curve at the final stage.

Discussion

Strain rate insensitivity has been deliberately assumed throughout this work. Dynamic testing is indeed aimed at assessing the effect of strain rate on the mechanical behav-

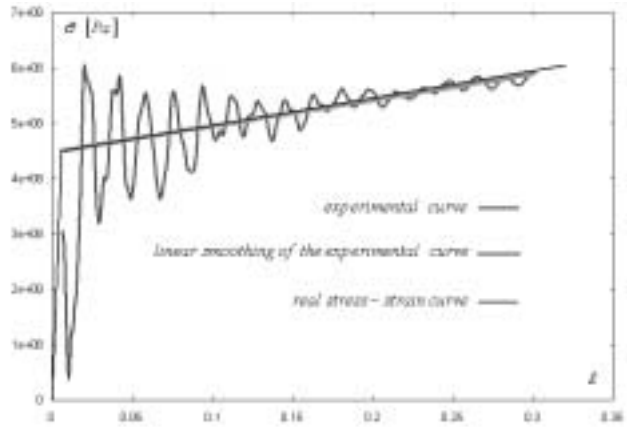

Fig. 14—Comparison between the linear approximation of the oscillating $\hat{\sigma}_{eqv} - \hat{\varepsilon}_{eqv}$ curve obtained by using the quasi-static k and eqs (10) and (11) in Part I[12] to the real $\hat{\sigma}_{eqv} - \hat{\varepsilon}_{eqv}$ curve

ior of materials. While this effect could be easily taken into account numerically, rate insensitivity was assumed to assess the accuracy of the method and the calculations, with respect to a fixed stress–strain relationship.

For both quasi-static and dynamic loading cases, the analyses reveal that the averaged $\hat{\varepsilon}_{eqv} - \hat{\sigma}_{eqv}$ on the mid-section reproduces the constitutive bilinear equation of the material. This result is not influenced by the yield stresses, specimen geometry (gage height, root radius) or strain rate. This result is backed by the observation that the stress and strain distribution in the gage section of the specimen is reasonably homogeneous, regardless of the loading rate. Previous work[9] had not addressed this important issue. This result is directly related to the smoothness of the $\hat{\sigma}_{eqv} - \hat{\varepsilon}_{eqv}$ curve, or in other words to the fact that a state of dynamic equilibrium is rapidly established over the gage section. This point is analogous to equilibrium requirements in a cylindrical specimen tested in the split Hopkinson pressure bar. In addition, one can notice the similarity of the SCS to the specimen used in pressure–shear experiments at very high strain rates[4] for which the present observation applies most likely.

The strain rate was found to be quite constant throughout the test, despite large oscillations in the measured load. This important result is consistent with another result showing that the stress–strain relationship is quite smooth in the gage section.

The previously unaddressed effects of friction at the end-pieces of the specimen were investigated for the dynamic loading case. Such effects are known to be important in conventional Kolsky bar testing of small cylinders and should naturally be assessed for the SCS. Two extreme cases, frictionless (contact with slip conditions) and frictional (contact with stick conditions), were investigated, as representative of lower and upper bounds, respectively. The resulting load was found to be slightly affected by frictional effects, as expected, but the latter do not affect significantly the stress–strain distribution in the gage section, and this is an important point from an experimental point of view. Yet, additional, information can be drawn from observing of the shape of the deformed specimen. Indeed, all experiments to date show a significant amount of lateral motion of the SCS end-pieces.[9–11] By comparing this observation to the deformed shape of a frictional SCS, it clearly seems that friction is not playing a significant role in the test.

The simple relationship originally proposed by Rittel et al.,[9,10] as expressed in eqs (10) and (11) of Part I,[12] was further verified in this work, and can now be simply established for any material and gage geometry. The applicability of the quasi-static procedure to the dynamic case has been used in previous work,[11] assuming its validity by means of experimentation. Here, the validity of this assumption is demonstrated numerically. However, one should note that a certain approximation is made, as follows. In the case of a strain-rate sensitive material, the plastic modulus will be affected, whereas in the suggested analysis, the same k_i coefficients are used, whereas they are related to some extent to the actual plastic modulus, as shown in Part I[12] of this investigation. The degree of influence is related to the plastic modulus itself, mostly for k_2 and k_3. However, it was found that these coefficients are almost unaffected by the material properties and gage width, when the latter is wider (Table 3 in Part I[12]). Therefore, the best accuracy will be obtained when testing "large" gage specimens (e.g. w = 2 mm). The average strain rate is dictated by k_3, so that prior knowledge on the anticipated plastic properties will be useful in planning the experiments for an anticipated strain rate. Keeping in mind the above-mentioned points, this relationship is of huge practical interest, and is the first of its kind for such a shear specimen.

Finally, the present work confirms that the SCS geometry can confidently be used, in a seamless manner, for the characterization of large strain behavior of materials over a wide range of strain rates.

Conclusions

The SCS has been analyzed numerically for dynamic loading conditions. Bilinear material behavior has been assumed, as a first step for the present analysis. Specific issues that were not addressed previously have been investigated, and the following conclusions can be drawn from the present work.

- The stresses and strains are quite homogeneous in the gage section.
- Frictional effects at the end-pieces of the specimen indeed exist but are of negligible influence for the determination of the mechanical properties (since slip conditions prevail in the experiments).
- The average strain rate is quite constant throughout the dynamic test.
- The simple relations, based on three coefficients, that were developed to reduce the $P-d$ curve into an equivalent stress–strain relationship for quasi static loading, can be used also for dynamic loading.
- Additional work should be carried out to include other types of material behavior, such as parabolic.

Acknowledgments

Support of the Lady Davis Postdoctoral Fund at Technion to AD is acknowledged. DR acknowledges the partial support of the Fund for Promotion of Research at Technion (grant

030-168). Useful discussions with G. Ravichandran and M. Vural are gratefully acknowledged.

References

1. Kolsky, H., "An Investigation of the Mechanical Properties of Materials at Very High Rates of Loading," Proceedings of the Physical Society of London, **62B**, *676–700 (1949).*

2. Kajberg, J., Sundin, K.G., Melin, L.G., and Ståhle, P., "High Strain-rate Tensile Testing and Viscoplastic Parameter Identification Using Microscopic High-speed Photography," International Journal of Plasticity, **20** *(4–5), 561–575 (2004).*

3. Rusinek, A. and Klepaczko, J.R., "Shear Testing of a Thin Sheet at Wide Range of Strain Rates and a Constitutive Relation with Strain-rate and Temperature Dependence of the Flow Stress," International Journal of Plasticity, **17** *(1), 87–115(2001).*

4. Clifton, R.J. and Klopp, R.W., Metals Handbook: Mechanical Testing, Vol. 8, ASTM, Metals Park, OH (1986).

5. Gilat, A. and Cheng, C.S., "Modeling Torsional Split Hopkinson Bar Tests at Strain Rates above 10,000 s^{-1}*," International Journal of Plasticity,* **18** *(5–6), 787–799 (2002).*

6. Meyer, L.W. and Manwaring, S., Metallurgical Applications of Shock Wave and High Strain Rate Phenomena, L.E. Murr et al., editors, Marcel Dekker, New York (1986).

7. Klepaczko, J.R., "An Experimental Technique for Shear Testing at High and Very High Strain Rates," International Journal of Impact Engineering, **46**, *25–39 (1994).*

8. Roessig, K.M. and Mason, J.J., "Adiabatic Shear Localization in the Dynamic Punch Test. Part II: Numerical Simulations," International Journal of Plasticity, **15** *(3), 263–283(1999).*

9. Rittel, D., Ravichandran, G., and Lee, S., "A Shear Compression Specimen for Large Strain Testing," EXPERIMENTAL MECHANICS, **42** *(1), 58−64 (2002).*

10. Rittel, D., Ravichandran, G., and Lee, S., "Large Strain Constitutive Behavior of OFHC Copper over a Wide Range of Strain Rates Using the Shear Compression Specimen," Mechanics of Materials, **34** *(10), 627−642 (2002).*

11. Vural, M., Rittel, D., and Ravichandran, G., "Large Strain Mechanical Behavior of 1018 Cold Rolled Steel over a Wide Range of Strain Rates," Metallurgical and Material Transactions A, **34A** *(12), 2873–2885 (2003).*

12. Dorogoy, A. and Rittel, D., "Numerical Validation of the Shear Compression Specimen. Part I: Quasi-static Large Strain Testing," EXPERIMENTAL MECHANICS, **45**.

13. Bathe, K.J., Finite Element Procedures in Engineering Analysis, Prentice-Hall, Englewood Cliffs, NJ (1982).